Conformationally Gated Metal Uptake by Apomanganese Superoxide Dismutase[†]

Mei M. Whittaker and James W. Whittaker*

Department of Science and Engineering, School of Medicine, Oregon Health and Science University, 20000 Northwest Walker Road, Beaverton, Oregon 97006-8921

Received August 18, 2008; Revised Manuscript Received September 3, 2008

ABSTRACT: Metal uptake by apomanganese superoxide dismutase in vitro is a complex process exhibiting multiphase "gated" reaction kinetics and a striking sigmoidal temperature profile that has led to a model of conformationally gated metal binding, requiring conversion between "closed" and "open" forms. This work systematically explores the structural determinants of metal binding in both wild-type (WT) apoprotein and mutational variants as a test of mechanistic models. The pH dependence of metalation under physiological conditions (37 °C) shows it is linked to ionization of a single proton with a pK_a of 7.7. Size exclusion chromatography demonstrates that the apoprotein is dimeric even when it is fully converted to the open form. The role of molecular motions in metal binding has been probed by using disulfide engineering to introduce covalent constraints into the protein. While restricting motion at domain interfaces has no effect, constraining the subunit interface significantly perturbs metal uptake but does not prevent the process. Mutagenesis of residues in the active site environment results in a dramatic shift in the transition temperature by as much as 20 °C or a loss of pH sensitivity. On the basis of these results, a mechanism for metal uptake by manganese superoxide dismutase involving reorientation of active site residues to form a metal entry channel is proposed.

Insertion of the catalytic metal is an essential step in the maturation of every metalloenzyme, yet in spite of its importance, relatively little is known about this aspect of metalloprotein function. A combination of in vivo and in vitro studies suggests that a variety of metalation mechanisms have evolved in biology (*1*), ranging from chaperoned delivery of toxic metal ions (Cu and Ni) (*1*−*3*) or complex metalloclusters (Fe−S) (*4, 5*) to simple reversible binding of metal cofactors (e.g., Ca and Mg) (*6*). These studies are just beginning, and the mechanism of metal binding is completely unknown for the majority of metalloenzymes.

Manganese superoxide dismutase (MnSOD) is an antioxidant metalloenzyme that serves as a front-line defense against oxidative stress (*7, 8*). It is a member of the highly conserved and ubiquitous (Mn,Fe)-SOD superfamily of enzymes, present in virtually all aerobic organisms and differing essentially only in their specific metal cofactor requirement (Mn or Fe) (*7*−*9*). Metal binding by SOD[1] is particularly important because the presence of the metal cofactor is required for catalysis, but binding the wrong metal ion may have toxic effects (*10*). The proteins are symmetric dimers (*11*) [or tetramers (*12*)] formed from identical subunits that are in turn based on a two-domain architecture (including an N-terminal α-hairpin domain, residues 1−99, and a C-terminal α/β-domain, residues 100−206, with EC MnSOD numbering), with a metal binding site buried in the interior of the protein, surrounded by a second shell of residues on all sides (Figure 1). In the holoprotein, the metal ion is ligated by amino acid side chains (His and Asp) arising from both N- and C-terminal regions, effectively cross-linking the two domains. Metal binding by *Escherichia coli* MnSOD has been shown to be moderately strong, but kinetically irreversible as a result of large protein activation barriers (*14*). The binding of distinct metal ions (e.g., Mn^{2+} and Co^{2+}) is mutually exclusive and kinetically competitive, indicating that there is a single high-affinity binding site in each subunit. Curiously, the apoprotein (prepared by chelation of the bound metal under denaturing conditions) is unable to rebind metal under ambient conditions (*15*). This observation initially led to the conclusion that the binding site of the renatured protein was occupied by an adventitious metal ion (*16*). We have recently shown that apo-MnSOD, while unable to bind metal at room temperature, undergoes a cooperative, thermally induced transition that allows metals to bind from solution (*17*−*19*). Conversion of apo-MnSOD to a form capable of binding metal ions occurs over a narrow temperature range for both mesophilic and thermophilic SOD apoproteins, but the midpoint temperature for the transition varies, typically lying near the optimal growth temperature of the source organism.

Recently, a direct continuous fluorimetic assay has been developed for assessing metal binding by apo-MnSOD based on quenching of intrinsic tryptophan luminescence when Co^{2+} ion binds in the active site (*19*). Analysis of the metal binding mechanism of *E. coli* apo-MnSOD by this method reveals kinetic behavior consistent with conformationally gated metal binding with the protein converting between

[†] This work was supported by the National Institutes of Health (Grant GM42680 to J.W.W.).

* To whom correspondence should be addressed. Telephone: (503) 748-1065. Fax: (503) 748-1464. E-mail: jim@ebs.ogi.edu.

[1] Abbreviations: EC, *Escherichia coli*; SOD, superoxide dismutase; IBA, 2-iodosobenzoic acid; bBm, bis-bromobimane [3,7-dimethyl-4,6-di(bromomethyl)-1,5-diazabicyclo[3.3.0]octa-3,6-dien-2,8-dione]; 2-ME, 2-mercaptoethanol; GnHCl, guanidinium hydrochloride; SEC, size exclusion chromatography; DTNB, 5,5-dithiobis(2-nitrobenzoic acid); EDTA, ethylenediaminetetraacetic acid.

10.1021/bi8015636 CCC: $40.75 © 2008 American Chemical Society
Published on Web 10/09/2008

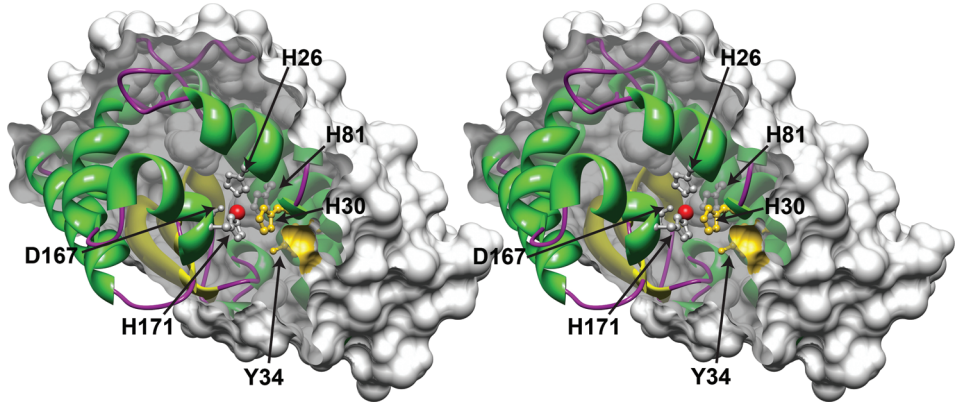

FIGURE 1: Buried metal binding site in manganese superoxide dismutase. A stereoview cross section through a single subunit of homodimeric EC MnSOD is shown, with a surface clipping plane bisecting the Mn coordination polyhedron. The solvent-excluded molecular surface of the protein is displayed (probe radius, 1.4 Å). The bound Mn ion (red sphere) and metal-ligating amino acid side chains (white, His26, His81, Asp167, and His171) as well as substrate gateway residues (yellow, His30 and Tyr34) are rendered as ball-and-stick structures using Chimera (*13*). Based on Protein Data Bank (PDB) entry 1vew.

Scheme 1: Conformationally Gated Metal Uptake by MnSOD

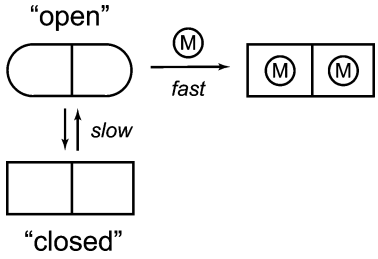

"open" and "closed" states, ion accessibility being defined empirically in terms of the metal uptake assay (Scheme 1). This gating process must reflect a conformational change associated with one of the protein interfaces, making the buried binding site accessible to metal ions in solution. The structure of the open state of apo-MnSOD is unknown at present. The X-ray crystal structure of a hyperthermophilic SOD apoprotein (from *Pyrobaculum aerophilum*), lacking bound metal ion, is virtually identical to the metallated form, but the structure presumably represents the closed state of the apoprotein (*20, 21*). Two models previously proposed for the open state (subunit dissociation and domain separation) (*19*) both involve large-scale reorganization of the protein structure, a requirement that has never been tested experimentally. This study uses protein mutagenesis to test both open state models and to probe the structural basis of the gating transition required for metal uptake by apomanganese superoxide dismutase.

MATERIALS AND METHODS

Biochemical Materials. All reagents were from commercial sources and used without purification.

Culture Media. Terrific Broth (TB) (12 g/L tryptone, 24 g/L yeast extract, 2.31 g/L potassium phosphate monobasic, and 12.54 g/L potassium phosphate dibasic), Luria-Bertani medium (LB) (5 g/L NaCl, 5 g/L yeast extract, and 10 g/L tryptone), and yeast-peptone-dextrose (YPD) (10 g/L yeast extract, 20 g/L peptone, and 20 g/L glucose), supplemented with antibiotics as required for selection (100 mg/L carbenicillin and 25 mg/L chloramphenicol), were used. Super Optimal Broth (SOB) (0.5 g/L NaCl, 2.5 mL of 1 mg/L KCl, 1.2 g/L $MgSO_4$, 5 g/L yeast extract, and 20 g/L tryptone) and SOC (SOB supplemented with 3 g/L glucose) were also used.

Biological Material. Ultracompetent *E. coli* XL2-Blue cells were from Stratagene (La Jolla, CA). Electrocompetent *E. coli* cells of other strains were routinely prepared by standard procedures (*22*) and electrotransformed using an Eppendorf 2510 electoporator with a 1 mm cuvette (18 kV/cm).

Construction of the E. coli ΔsodA Expression Host. An *E. coli* Δ*sodA* deletion strain was constructed for MnSOD protein expression, using phage λ Red recombineering methods (*23, 24*). *E. coli* BW25113 and pKD3, pKD43, and pCP20 plasmids were obtained from F. Wayne Outten (University of South Carolina, Columbia, SC). DNA for *sodA* gene deletion was prepared using oligos REDSOD1−6 (Table 1) with pKD3 and pQGBsodA (*18, 25*) as templates. After the reaction, the PCR mixtures were treated with *Dpn*I restriction enzyme to digest the templates and subsequently heated to 65 °C to inactivate the restriction enzyme. Separate PCR products for the *sodA* 5′ and 3′ genomic flanking regions and the CAT (Cm^R) insert were joined by overlap extension, and the resulting 1320 bp product was used to transform electrocompetent *E. coli* BW25113 | pKD43 grown in SOB overnight with L-arabinose and carbenicillin. Transformants were recovered in SOC medium and spread on LB/Cm plates for selection. Positive clones were subsequently screened by colony PCR using primers specific for the *sodA* coding region. One of these clones was made electrocompetent, transformed with pCP20, and selected on LB/C agar at 30 °C. Single colonies were streaked onto YPD nonselective media and grown at the nonpermissive temperature (43 °C) to cure the pCP20 plasmid. Single colonies were subsequently cleaned by restreaking and cultivation at 37 °C, and the Δ*sodA* genotype was verified by PCR using genomic DNA as the template.

Construction of the pBAD2sodA Expression Vector. The commercially available expression vector pBAD/gIII-A (Invitrogen, Carlsbad, CA) was modified for MnSOD expression, eliminating two *Nde*I restriction sites (one flanking the pBR322 ori region of the vector and a second *Nde*I restriction site within the multilinker) and introducing a new *Nde*I restriction site at the translational initiation site under the P_{BAD} promoter by triple mutagenesis using the mutagenic

Table 1: Oligonucleotides Used in This Work

name	sequence
RED-SOD-1	5′-GGGCATTTTCCTGCAAAAC-3′
RED-SOD-2	5′-ACCACATCAATTGAAACGCTG-3′
RED-SOD-3	5′-GAAGCAGCTCCAGCCTACACCCAGTATTGTCGGGCGG-3′
RED-SOD-4	5′-GGACCATGGCTGATTCCCATGCATTTGCCGCCTGCTG-3′
RED-SOD-5	5′-CCGCCCGACAATACTGGGTGTAGGCTGGAGCTGCTTC-3′
RED-SOD-6	5′-CAGCAGGCGGCAAATGCATGGGAATTAGCCATGGTCC-3′
BAD-QC-1	5′-P-GGTATTTCACACCGCATAAGTGCACTCTCAGTACAATCTG-3′
BAD-QC-2	5′-P-GATCTGCAGCTGGTACCAAATGGGAATTCGAAGCTTTC-3′
BAD-QC-3	5′-P-GGGCTAACAGGAGGAATTACATATGAAAAAACTGCTGTTCGC-3′
S126C	5′-P-CGCTTTGGTTGCGGCTGGGCATGG-3′
Y174C	5′-P-GTGGGAACATGCTTACTGCTTGAAATTCCAGAACCGC-3′
E170C	5′-P-GCCTGGATGTGTGGTGCCATGCTTACTACTTGAAATTC-3′
R72C	5′-P-GAAAACCGTACTGTGCAACAACGCTGGC-3′
D147C	5′-P-CTACTGCTAACCAGTGTTCTCCGCTGATGGG-3′
H17C	5′-P-ACGATGCCCTGGAACCGTGTTTCGATAAGCAGACCA-3′
N190C	5′-P-AAAGAGTTCTGGTGCGTGGTTAACTGGGACGAAGCAG-3′
H171A	5′-P-GCCTGGATGTGTGGGAAGCTGCTTACTACCTGAA-3′

oligos BAD-QC-1, -2, and -3 (Table 1) and the Quik-Change Multi mutagenesis kit (Stratagene, La Jolla, CA). The pBAD2 product was verified by restriction mapping and/or nucleotide sequence analysis. The *sodA* coding sequence obtained by *Nde*I and *Hin*dIII digestion of the pQGBsodA plasmid (*18, 25*) was ligated to a similarly digested pBAD2 vector to form pBAD2sodA.

Site-Directed Mutagenesis. Mutational variants of EC MnSOD were prepared by site-directed mutagenesis of the pBAD2sodA expression plasmid template, using the Quik-Change Multi mutagenesis kit (Stratagene) and the appropriate oligonucleotide primers (Table 1). The sequences of the products were verified by direct sequence analysis (Molecular Biology Core Sequencing Facility, Oregon Health and Science University). Plasmids were transformed into electrocompetent *E. coli* BW25113 Δ*sodA* cells for expression.

Recombinant Protein Expression. E. coli BW25113 Δ*sodA* | pBAD2sodA expression strains were inoculated into 1 L of Terrific Broth (TB) supplemented with 2 g/L glucose and 100 mg/L carbenicillin and grown to saturation at 37 °C with shaking. The cells were collected and resuspended in 1 L of TB (without phosphate) supplemented with 5 mM $MnCl_2$, 2 g/L glycerol, and 0.5 g/L L-arabinose. Cells were harvested after being incubated at 37 °C for 24 h with shaking. EC MnSOD H30A, Y34A, Y34F, E170A, and Y174F variants were expressed as previously described (*26*−*29*).

Protein Purification. EC MnSOD was purified by a modification of previously described methods (*26*). The cell-free extract from 15 g of cells was loaded onto an ion exchange column (DE-52, 5 cm × 45 cm), and the flow-through SOD fractions were further purified by CM-52 chromatography or chromatofocusing (PBE-94 Polybuffer Exchanger developed with Polybuffer-74 ampholyte).

Formation of the Apoprotein. Metal-containing MnSOD was denatured in 3.5 M guanidinium HCl (GnHCl) (pH 3.5) containing 10 mM EDTA and renatured by dialysis against 20 mM Tris/EDTA (pH 7.6) (*15, 30*). EDTA was removed by gel filtration (BioGel P-6). For thiol-containing variants, 2-mercaptoethanol (2-ME) was included when required to prevent disulfide formation. The apoprotein product was stored at −80 °C.

Metal Reconstitution. Apo-MnSOD (approximately 0.2 mM) in 40 mM MOPS (pH 7.8) containing 8 mM $MnCl_2$ was incubated at 37 °C for 0.5−2 h. After being cooled on ice, the solution was made 8 mM in EDTA and desalted by gel filtration (BioGel P-30) in 20 mM potassium phosphate buffer (pH 7). These reconstituted samples were used for Mn analysis and superoxide dismutase activity assays. Some samples were reconstituted by denaturation and renaturation in GnHCl as described above for preparation of the apoprotein, without EDTA and with 1 mM $MnCl_2$.

Fluorimetric Metal Uptake Assay. Metal uptake measurements were performed using a Cary Eclipse spectrofluorimeter (Varian, Inc., Walnut Creek, CA) equipped with a Cary temperature controller and a Peltier four-position multicell holder. Protein samples (50 μg/mL in 20 mM MOPS or TAPS buffer) were excited at 280 nm, and the emission intensity was monitored at 333 nm using a dynode voltage of 650 V. Metal binding time courses were initiated by adding an aliquot of a 6 mM $CoCl_2$ stock solution to a thermally equilibrated, stirred solution of apo-MnSOD to give a final Co^{2+} concentration of 24 μM (10 equiv). Both the protein sample and the metal stock solution were equilibrated at the target temperature for 7 min before the reaction was started. Fluorescence emission intensity was recorded at a sampling frequency of 1 s^{-1} for 30 min after addition of metal salts. The kinetic time courses were imported into a data analysis program (Scientist, Micromath Research, St. Louis, MO) and fit to a multiexponential relaxation process, including two exponential relaxation phases, a linear time-dependent term, and a constant offset (*19*).

Protein Characterization. The concentration of purified SOD was determined by optical absorption measurements, using the published molar extinction coefficient ($\varepsilon_{280} = 8.66 \times 10^4$ M^{-1} cm^{-1}) (*31*) or by the method of Lowry et al. (*32*). Superoxide dismutase activity was measured with the xanthine oxidase/cytochrome *c* inhibition assay (*33*). Metal analyses were performed using a Varian Instruments SpectrAA model 20B atomic absorption spectrometer equipped with a GTA 96 graphite furnace.

Protein homogeneity was routinely evaluated using SDS−PAGE. Nonreducing discontinuous SDS−PAGE was performed using 12% Tris-HCl Ready-Gel (Bio-Rad Laboratories, Hercules, CA) to detect formation of covalent cross-links. For reducing SDS−PAGE, 5% 2-ME was included in the sample buffer.

Protein quaternary structure was determined by size exclusion chromatography (SEC) over BioGel P-100 or Sephacryl 100-HR (1.5 cm × 100 cm) in a thermostated column with the temperature controlled by a circulating water

bath. For measurement of the SOD apoprotein, the elution buffer contained 1 mM EDTA and the metal-free character of the sample was verified by fluorimetric metal uptake after gel filtration.

Quantitation of free thiols was performed by reaction of protein samples with Ellman's reagent [5,5′-dithiobis(2-nitrobenzoic acid) (DTNB)] with or without 4 M GnHCl, monitoring product formation at 412 nm according to the published procedure (*34*). The analysis was calibrated using the L-cysteine standard.

Thiol Oxidation. Protein thiols were oxidized by treating the protein (0.2 mM) in 100 mM potassium phosphate buffer (pH 7.8) containing 1 mM EDTA with 1.2 equiv (relative to free SH) of 2-iodosobenzoic acid (IBA) (*35*) for 24 h at room temperature followed by desalting (Bio-Gel P-6). The extent of the reaction was determined by nonreducing SDS−PAGE analysis, and the free thiol content of the product was determined by reaction with DTNB.

Bis-Bromobimane Covalent Bridge Modification. Apo-MnSOD (R72C/D147C) (0.5 mM) in 50 mM HEPES (pH 7.5) containing 4 mM EDTA was reacted with bis-bromobimane (bBm) (*36*) (1.5 equiv) at 37 °C for 1 h. The mixture was centrifuged and desalted (BioGel P-6) in the dark. The product of the reaction was analyzed by reaction with DTNB and a sample prepared by extensive dialysis against ammonium acetate buffer and water for mass spectrometry.

Mass Analysis. Mass analysis was performed by the Proteomics Shared Resource (Oregon Health and Science University). Prior to mass analysis, samples were mixed 1:1 with a solution of 49.9% acetonitrile, 49.9% deionized water, and 0.2% formic acid. Samples were then infused into an Applied Biosystems QSTAR XL mass spectrometer with an electrospray ionization source using a syringe pump at a flow rate of 10 μL/min. The resulting mass spectrum was deconvoluted using the Bayesian Protein Reconstruct utility of the Bioanalyst extensions module for Analyst QS 1.1.

RESULTS AND DISCUSSION

Biochemical Characterization of the Gating Transition. The biphasic kinetics that have been previously reported for metal uptake by apo-MnSOD (*19*) imply that metal binding is a conformationally gated, sequential process in which the rate-limiting step is a structural change and not the intrinsic metal binding reaction. In this process, the protein interconverts between the reactive (open gate) and nonreactive (closed gate) conformations (Scheme 1) in a two-state dynamic equilibrium, as demonstrated in earlier temperature dependence studies. The fraction of open form present in the equilibrium mixture is reflected in the ratio of the fast phase amplitude to the total amplitude (sum of fast and slow phase amplitudes) (A_0/A_{TOT}) (Figure 2, inset).

The earlier studies have been extended to investigate the pH sensitivity of the apo-MnSOD metalation process by performing the fluorimetric metal uptake assay in buffers spanning a range of pH values (6.5−8.5) at a constant temperature (37 °C). The open fraction (A_0/A_{TOT}) increases from <0.2 to>0.8 over this pH range, reflecting extensive conversion to the open form of the protein at higher pH (Figure 2). The data were fit to a modified Henderson−Hasselbalch equation for a pH-dependent equilibrium (eq 1), including a Hill coefficient (n) to model titration of interacting sites (*37*):

$$A_0/A_{TOT} = 10^{n(pH-pK_a)}/[1 + 10^{n(pH-pK_a)}] \quad (1)$$

This analysis yields an apparent pK_a of 7.7 for the pH-dependent process and a Hill coefficient (n) of 0.7 (Figure 2, top). The magnitude of the Hill coefficient suggests that interaction with a second site titrating over this pH range gives rise to a modest anticooperativity for the deprotonation event governing the metal uptake kinetics.

As expected, the rate constant associated with the slow phase (k_{slow}) is also pH-dependent. The pH sensitivity of the kinetics arises from a hydrogen ion ([H$^+$]) term in the underlying empirical rate law, leading to expressions that allow proton ionization steps to be detected through the pH dependence of the rate constant (*38*) (eqs 2 and 3):

$$k = c[H^+]^m \quad (2)$$

$$\log k = \log c - m \times pH \quad (3)$$

Equation 3 describes a log-linear pH−rate relation, with a slope ($-m$) whose sign (plus or minus) indicates whether the transition state involves proton loss or gain, respectively, and whose magnitude may be interpreted as the number of protons actively involved in the transition state for the rate process. In this case, the data exhibit a clear a log-linear rate profile with a slope ($-m = 1.1$) reflecting ionization of a single proton in the closed → open transition (Figure 2, bottom).

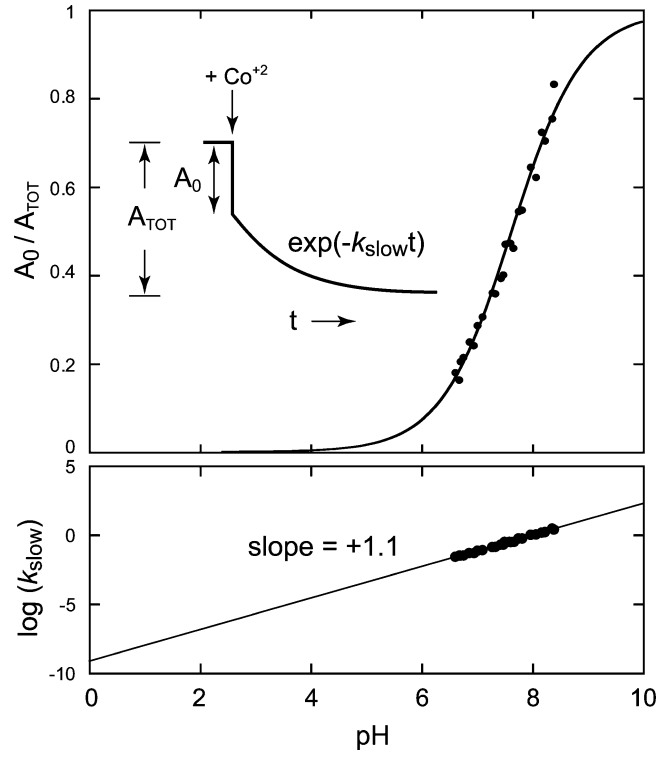

FIGURE 2: pH dependence of metal binding by Apo-MnSOD. Co^{2+} uptake was monitored fluorimetrically as described in Materials and Methods. MnSOD (50 μg/mL) in 2.5 mL of sample buffer was equilibrated at 37 °C for 7 min, and the reaction was initiated by addition of 24 μM $CoCl_2$ (approximately 10 stoichiometric equivalents). The pH of each sample was measured directly in the reaction cuvette. The top panel shows the pH dependence of the fast phase gating fraction (A_0/A_{TOT}). A fit of the data to a modified Henderson−Hasselbalch equation as described in the text is shown (pK_a = 7.7). The bottom panel shows the pH dependence of the slow phase rate constant, k_{slow}. A linear fit to the data is shown ($-m$ = 1.1).

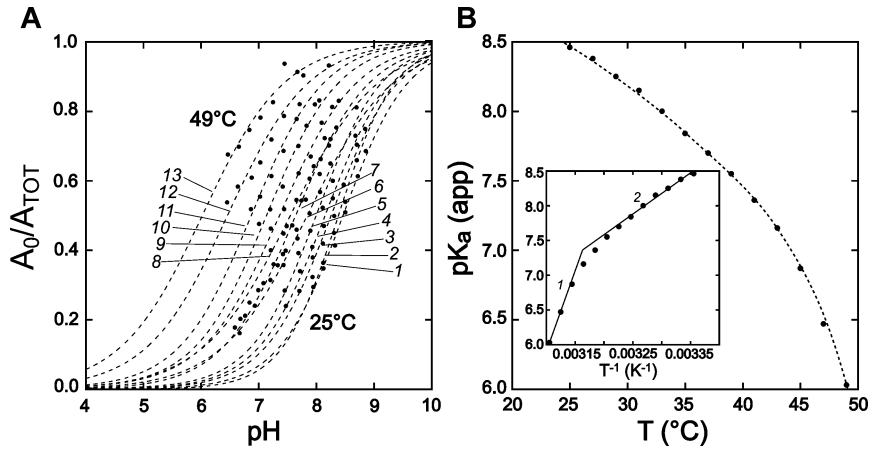

FIGURE 3: Temperature dependence of the apo-MnSOD gating equilibrium. (A) pH titration isotherms measured for Co^{2+} uptake by apo-MnSOD at 25−49 °C at 2 °C intervals (*1*−*13*). Data were fit to a modified Henderson−Hasselbalch equation as described in the text, and the fitted lines are shown. (B) Apparent pK_a values for metal uptake determined for temperatures ranging from 25 to 49 °C are shown with a polynomial fit to guide the eye. The inset shows van't Hoff analysis of the temperature-dependent apparent pK_a for the gating transition. van't Hoff parameters: (1) high-temperature limit, $\Delta H_{vH} = 160$ kJ/mol, $\Delta S_{vH} = 450$ J mol^{-1} K^{-1}; (2) low-temperature limit, $\Delta H_{vH} = 70$ kJ/mol, $\Delta S_{vH} = 164$ J mol^{-1} K^{-1}.

Repeating the pH profile measurement over a range of temperatures (25−49 °C) reveals a coupling between protonation and the temperature dependence of gating equilibria in the protein (Figure 3). Titration isotherms recorded at different temperatures are dramatically shifted, yielding very different values of the apparent pK_a for metal uptake (9 vs 6) at the low- and high-temperature limits of the range. These results imply that metal uptake is facilitated by deprotonation of a site in the protein, while increasing the temperature permits metal uptake to occur at lower pH by increasing the level of thermal excitation.

The combination of the pH dependence of the open fraction in the fast phase and the log-linear pH−rate profile provides evidence of an essential single proton ionization step in the conformational gating transition, associated with a group having an apparent pK_a of 7.7 at 37 °C. On the basis of published values for intrinsic pK_a values of protein constituents (*39*), the apparent pK_a of 6 observed at temperatures approaching the global unfolding temperature of apo-MnSOD ($T_m = 52$ °C) (*14*) is in the range typical of solvent-exposed His side chains in proteins. At lower temperatures, the apparent pK_a increases to values consistent with His in a salt bridge (e.g., carboxylate complex) (*40, 41*). The temperature dependence of the apparent pK_a suggests a decrease in the strength of the salt bridge at elevated temperatures. While these results appear to implicate a His residue in the gating transition, it does not specify which of the eight His residues in EC MnSOD are involved, or the nature of the conformational gating process.

A van't Hoff analysis of the data (Figure 3, inset) allows the temperature dependence of the apparent pK_a to be interpreted in terms of thermodynamic parameters. The limiting slope at a low temperature (25 °C) yields estimates for ΔH_{vH} and ΔS_{vH} of 70 kJ/mol and 164 J mol^{-1} K^{-1}, respectively, and at a high temperature (45 °C) estimates for ΔH_{vH} and ΔS_{vH} of 160 kJ/mol and 450 J mol^{-1} K^{-1}. The latter results are similar to those previously obtained from analysis of the temperature dependence of the gating equilibrium at a constant pH (7.0).

The sensitivity of the gating transition to both temperature and pH has made it possible to identify experimental conditions (pH 7.5 and 45 °C) under which the apoprotein is fully converted to the open state. Analysis of the protein under these conditions should allow the structural basis for the conformational gating to be defined. Specifically, it suggests a critical test of a requirement for dissociation of the subunits in the gating transition.

Size exclusion chromatography (SEC) apo-MnSOD in 20 mM MOPS buffer (pH 7.5) containing 1 mM EDTA at 45 °C [or 20 mM TAPS buffer (pH 9) at room temperature] indicates that under these conditions the protein remains dimeric, with no significant dissociation of the subunits, although elution of the apoprotein is delayed slightly compared to that of the Mn_2-MnSOD holoprotein (Figure 4). Under the same conditions, the MnSOD E170A variant, which has previously been shown to extensively dissociate in solution (*26*), is found to be purely monomeric by SEC (Figure 4). These results appear to exclude subunit dissociation as a requirement for conversion to the open state. However, the subunit dissociation model can be tested even more stringently by introducing covalent constraints into the protein structure (see below).

Engineering Disulfide Constraints. Two models previously proposed for the conformational gating transition of apo-MnSOD (subunit dissociation and domain separation) both require the folded protein to open up at specific molecular interfaces. One way to experimentally test whether displacement at an interface is involved in metal uptake is to constrain the interface with a covalent cross-link and measure the effect on the process. The absence of cysteine residues in WT EC MnSOD suggests the possibility of performing Cys substitution mutagenesis to constrain the structure with disulfides, an approach that has proven effective in probing molecular motions in other proteins (*42*−*44*).

To implement this strategy, it is first necessary to identify residues that should readily form unstrained disulfides in the protein when replaced with Cys residues. Structural studies suggest that C_β atoms in a protein disulfide should optimally be separated by 3.5−5 Å (*45, 46*), so residue pairs in EC MnSOD having C_β atoms within this separation range were identified by importing the C_β atomic coordinates for metallated EC Mn_2-MnSOD (PDB entry 1vew) into a

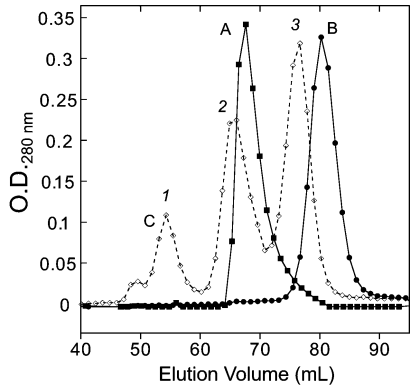

FIGURE 4: Size exclusion chromatography of apo-MnSOD. A thermostated column of BioGel P-100 (1.5 cm × 100 cm) equilibrated with 20 mM MOPS (pH 7.5) containing 1 mM EDTA at 45 °C was loaded with apo-MnSOD (trace A), Fe_2-MnSOD (E170A) (trace B), or a MW calibration mixture (trace C): (1) bovine serum albumin, (2) Mn_2-MnSOD, and (3) carbonic anhydrase.

spreadsheet analysis program (Microsoft EXCEL) and using the geometric constraint as a search criterion. The targets identified by this method include three residues on the symmetric dimer interface of the protein (Ser126, Glu170, and Tyr174) (Figure 5), where Cys substitution is predicted to allow disulfides to form with the corresponding residue in the opposing subunit, as well as a pair of residues (His17 and Asn190) whose replacement by Cys could serve to constrain the first helix of the N-terminal domain, which covers the metal binding site (Figure 5). On the basis of the selection criterion, no suitable residue pairs were found that could be used to introduce a disulfide constraint at the opposite end of the domain interface. However, an Arg−Asp salt bridge "clasp" feature (Arg72 and Asp147) that is highly conserved over MnSOD structures was selected as a starting point for constraining the domain motions through Cys engineering.

Each of the mutational variants was constructed by site-directed mutagenesis of the pBAD2sodA expression vector, which places the EC MnSOD gene under control of the tight, strong arabinose promoter (*47*), and the protein products were purified from a specially constructed expression host [a Δ*sodA* deletion strain of *E. coli* BW25113 created by phage λ Red recombineering methods (*23, 24*)] to preclude contamination with wild-type MnSOD. The pBAD2sodA expression vector has proven to be very efficient, routinely yielding > 250 mg of purified EC MnSOD protein from 15 g of cells in 1 L expression cultures under L-arabinose induction. The recombinant protein was purified by ion exchange and chomatofocusing chromatography.

Nonreducing denaturing electrophoresis (SDS−PAGE) was routinely used to evaluate the disulfide status of the protein, taking advantage of the distinct electrophoretic mobilities of thiol- and disulfide-containing forms. Subunit-bridging disulfides result in the denatured protein migrating at approximately twice the monomer mass, while more subtle changes are produced by intrachain disulfides. Linkage isomers of interchain disulfides also produce subtle variations in electrophoretic mobility that can be used to assign the site of the cross-link. For each sample, thiol quantitation by the DTNB assay was performed to determine the free sulfhydryl content of the purified protein. Most of the Cys variants were isolated as reduced, thiol-containing species, requiring oxidation to form the disulfide.

Iodosobenzoic acid (IBA) (*35*) was used to convert the thiol-containing protein to the disulfide form, as described in Materials and Methods. Depending on the specific variant (see below), IBA was added to either the metal-containing holoprotein or the apoprotein following metal extraction. The progress of the oxidation reaction was monitored by non-reducing SDS−PAGE. Following oxidation, excess IBA reagent was removed by desalting and the protein characterized by SDS−PAGE and DTNB analysis. The fluorimetric metal uptake assay (*19*) (see Materials and Methods) was used to evaluate the metal binding behavior of the variants (Figure 6).

(i) R72C/D147C. The domain separation model for Mn-SOD metal uptake was based on the observation that the metal binding site lies on the domain interface and that the contact surface between the two domains might permit them to open, making the binding site accessible to metal ions in solution. As noted above, screening C_β separations did not identify any pairs of residues appropriate for introducing a disulfide bond at this domain interface. However, two residues that form a clasp salt bridge between the domains (Arg72 and Asp147, for which a C_β separation of 7.2 Å is predicted) were selected as a starting point for constraining this region of the protein structure (Figure 5). Substitution of both of these residues with Cys yielded the MnSOD R72C/D147C variant, which, as expected, formed disulfides only under forcing conditions that resulted in polymerization of the protein. However, the predicted separation between SG sulfhydryls in the R72C/D147C variant (approximately 4.7 Å) is within the span predicted for a bifunctional sulfhydryl reagent, bis-bromobimane (bBm) (*36*) [3.17−6.61 Å (*48*)]. Formation of a covalent bridge between the Cys residues was monitored fluorimetrically, and the product was characterized by mass spectrometry (Table 2), nonreducing SDS−PAGE, and the DTNB assay (Table 3), confirming the presence of the cross-link and the absence of intermolecular cross-links. Metal uptake by apo-MnSOD (R72C/D147C/bBm) (Figure 6, trace 2) was essentially indistinguishable from that observed for the WT protein (Figure 6, trace 1), demonstrating that the clasp region of the domain interface is not directly involved in the metal uptake process. The high specific activity of the Mn derivative containing the bBm bridge (Table 3) also shows that the modification has little effect on the active site.

(ii) H17C/N190C. A second domain interface that might be involved in metal binding is formed by the contact between the first α-helix of the N-terminal domain (helix 1) and the C-terminal domain. Helix 1 donates one of the metal ligands (His26) as well as the two substrate gateway residues (His30 and Tyr34) to the active site structure, and separation of helix 1 from the C-terminal domain would open a path into the active site. To test the possible involvement of helix 1 motion in the metal uptake process, the helix was constrained by introducing Cys residues into the preceding turn (H17C) as well as into an adjacent C-terminal helix (N190C) (Figure 5). The relatively large C_β separation for this pair of residues (4.5 Å) makes it likely that a disulfide formed between them will be in an extended conformation, preventing separation of these structural elements. The apo-MnSOD (H17C/N190C) disulfide performed a metal uptake

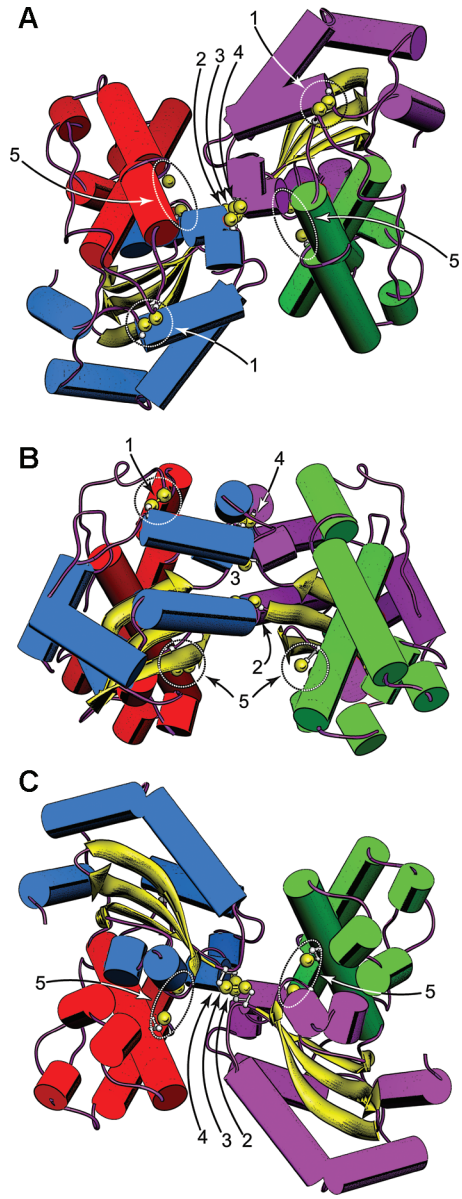

FIGURE 5: Disulfide constraints introduced into the EC MnSOD structure by Cys substitution mutagenesis. (A) Top view of the MnSOD dimer, parallel to the molecular 2-fold axis on the N-terminal domain side. (B) Side view of the MnSOD dimer, perpendicular to the molecular 2-fold axis. (C) Bottom view of the MnSOD dimer, parallel to the molecular 2-fold axis on the C-terminal domain side. The cysteines shown are hypothetical structures based on replacement of the corresponding residues in WT MnSOD (PDB entry 1vew) with Cys and manually adjustment of the side chain dihedrals. Cysteines are rendered with ball-and-stick side chains, with the Cys SG sulfur shown as a van der Waals sphere. In each view, the individual domains and subunits are identified by helix color. Subunit A: N-domain, green; C-domain, purple. Subunit B: N-domain, red; C-domain, blue. (1) H17C−N190C disulfide. (2) $S126C_A-S126C_B$ disulfide. (3) $E170C_A-E170C_B$ disulfide. (4) $Y174C_A-Y174C_B$ disulfide. (5) R72C, D147C pair. Rendered using Chimera (*13*).

reaction indistinguishable from that of the WT protein (Figure 6, trace 3), and the Mn complex is fully active (Table 3). The absence of any detectable perturbation of metal uptake by constraints restricting the domain interface at either end of the molecule provides a clear indication that domain separation is not required for metal binding by apo-MnSOD.

(iii) S126C. In WT MnSOD, Ser126 lies on the dimer interface close to the molecular 2-fold symmetry axis, the hydroxyl group forming a hydrogen bond with the corresponding residue in the opposing subunit (Figure 5). The Cys substitution variant EC MnSOD S126C was isolated as the free thiol form, which SEC shows is monomeric in solution (Table 3). Ionization of the opposing cysteine thiols on the subunit interface of this variant will generate a pair of thiolate anions, contributing to electrostatic destabilization of the dimer and possibly accounting for dissociation of the subunits. Metal uptake by apo-MnSOD S126C (SH) is very fast (Figure 6, trace 9), similar to that of apo-MnSOD E170A (Figure 6, trace 11) (see below), which is also monomeric (*26*). The product [Mn_2-MnSOD S126C (SH)] is predominantly dimeric in solution and has approximately 65% of the WT SOD activity (Table 3).

Oxidation of apo-MnSOD S126C by IBA proceeds smoothly, yielding the disulfide-cross-linked dimer. The homologous *Mycobacterium tuberculosis* FeSOD S123C variant, which has recently been reported (*49*), was also expressed in *E. coli* as a thiol form, although in that case the quaternary structure was not investigated. The thiol form of *M. tuberculosis* FeSOD S123C spontaneously oxidized to the disulfide during months-long crystallization in air, and X-ray crystallography confirmed that the presence of the Cys123 disulfide did not perturb the structure of the protein.

Metal uptake kinetics in the fluorimetric assay show a distinctly WT-like biphasic reaction progress curve for apo-MnSOD S126C (SS) (Figure 6, trace 8). Manganese is also stably bound, and Mn_2-MnSOD S126C (SS) exhibits 66% of the WT catalytic activity (Table 3). The Cys126 disulfide is a covalent cross-link that prevents separation of the subunits and constrains motion of the lower part of the subunit interface (Figure 5). Thus, metal uptake by apo-MnSOD S126C (SS) excludes complete dissociation of the subunits as a requirement for metal binding. However, in principle, partial separation of the subunit interface could still occur in this single-disulfide variant, with the disulfide serving as a pivot point.

(iv) Y174C. Apo-MnSOD Y174C (SS) disulfide, formed by metal extraction from purified EC MnSOD Y174C (SH), refolding, and oxidization by IBA, covalently cross-links the dimer across the subunit interface, at the opposite edge from the Cys126 disulfide (Figure 5). Replacement of Tyr174 with Cys also removes a residue that forms a conserved hydrogen bond to one of the gateway residues (His30) in WT MnSOD (Figure 1). Metal uptake by apo-MnSOD Y174C (SS) is monophasic and relatively slow (Figure 6, trace 13), indicating that metal binding is significantly perturbed in this variant but still proceeds, and the protein binds and retains the full complement of metal ion (Table 3). Metal uptake by the covalently cross-linked dimeric protein demonstrates that complete dissociation of the subunits is not required for metal binding. However, some restricted motion of the subunit interface may occur in the MnSOD Y174C disulfide, as noted above for the MnSOD S126C disulfide.

(v) S126C/Y174C. A dicysteine variant was constructed to more completely constrain motion at the subunit interface and exclude the possibility of a "butterfly" motion of the protein involving partial separation of the subunits. The two cysteines in this variant (Cys126 and Cys174) form a pair of disulfides with the corresponding residues in the opposing subunit, constraining the interface at opposite sides of the molecule (Figure 5).

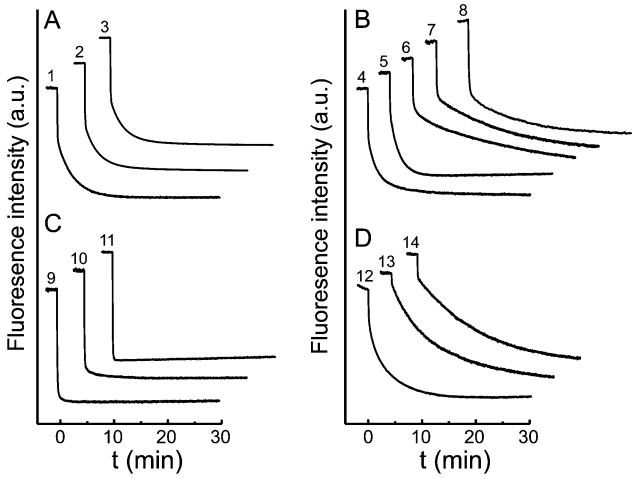

FIGURE 6: Representative metal uptake time courses for apo-MnSOD variants. Co^{2+} was added to apo-MnSOD (50 μg/mL in 20 mM MOPS) at time zero, and binding was assessed fluorimetrically as described in Materials and Methods. Reaction time courses for mutational variants are presented as a stack plot. Four distinct kinetic patterns are distinguished: (A) biphasic, indistinguishable from WT; (B) biphasic, distinct from WT; (C) monophasic, fast-reacting; and (D) monophasic, slow-reacting. Individual traces: (1) WT apo-MnSOD, 37 °C, pH 7.6; (2) apo-MnSOD (R72C/D174C/bBm), 37 °C, pH 7.6; (3) apo-MnSOD (H17C/N190C) (SS), 37 °C, pH 7.6; (4) apo-MnSOD H30A, 33 °C, pH 7.0; (5) apo-MnSOD Y174F, 37 °C, pH 7.6; (6) apo-MnSOD Y34A, 31 °C, pH 7.0; (7) apo-MnSOD Y34F, 23 °C, pH 7.0; (8) apo-MnSOD S126C (-SS-), 37 °C, pH 8.8; (9) apo-MnSOD S126C (SH), 25 °C, pH 7.6; (10) apo-MnSOD (S126C/Y174C) 2× (SS), 37 °C, pH 7.6; (11) apo-MnSOD E170A, 37 °C, pH 7.0; (12) apo-MnSOD E170C (SS), 37 °C, pH 7.6; (13) apo-MnSOD Y174C (SS), 37 °C, pH 7.6; and (14) apo-MnSOD H171A, 37 °C, pH 7.0.

Table 2: Mass Analysis of the MnSOD R72C/D147C Variant

	mass shift relative to WT MnSOD[a] (amu)	
molecular species	predicted	observed
R72C/D147C 2× (SH)	−66	−65
R72C/D147C/bBBm adduct[b]	+103	+101

[a] Determined by ESI-MS of the protein as described in Materials and Methods. [b] Prepared as described in Materials and Methods.

MnSOD S126C/Y174C was treated with IBA to form the double disulfide, from which metal extraction and refolding afforded apo-MnSOD S126C/Y174C 2× SS. The fluorimetric metal uptake assay demonstrates that this variant is able to bind Co^{2+} ion (Figure 6, trace 10), although the metal ion is relatively weakly bound and is lost during desalting in the presence of EDTA and denaturation and renaturation in the presence of metal ion (Table 3). The progress curve for the metal uptake reaction is consistent with a predominantly open form for this variant, and the inability of the protein to retain the metal ion might indicate that conversion to the closed metal complex is blocked.

(vi) E170C. Previous studies have demonstrated the importance of a conserved outer-sphere glutamate (Glu170) in the structure and function of the EC MnSOD active site (*26*). The salt bridge cross-link formed by Glu170 with the coordinating His171 in the opposing subunit is an important element stabilizing the dimeric organization of the protein, and replacement with alanine (MnSOD E170A) results in dissociation of the metallated protein into monomers and also appears to alter the metal binding selectivity of the apoprotein in vivo (*26*). Like Ser126 and Tyr174, Glu170 spans the midpoint of the subunit interface close to the molecular 2-fold symmetry axis, and replacement by Cys would be expected to stabilize the dimeric structure, forming a covalent disulfide cross-link between the Cys170 residues arising from opposing subunits (Figure 5).

MnSOD (E170C) was isolated as the metalated disulfide form following purification. Metal extraction and refolding afforded apo-MnSOD E170C SS disulfide. Metal binding is observed in the fluorimetric metal uptake assay, with essentially monophasic kinetics (Figure 6, trace 12) lacking pH dependence ($-m = -0.04$), suggesting that the site responsible for the proton sensitivity is severely perturbed in this variant. Approximately half of the bound metal appears to be lost during desalting in the presence of EDTA (Table 3). The relative stability of the half apo complex (compared to holo) may reflect the role of Glu170 as a charge-compensating outer-sphere counterion in the active site. Summing charges on the buried metal ion and its coordinating ligands leads to a +1 overall charge on the metal complex in SOD, which is normally balanced by the −1 charge provided by the Glu170 carboxylate in the outer sphere. However, in MnSOD E170C disulfide, this charge compensation is absent, and the two metal cations in adjacent

Table 3: Properties of EC MnSOD Cysteine Variants

variant	free SH[a] (mol of SH/mol of protein)	thiol status	metalation state	specific activity (units/mg)	quaternary structure	Mn content	metal uptake[h]
S126C	0.99	SH	apo[b]	−	monomer[f]		+
			Mn[c]	4815 ± 232 (66%)[e]	dimer[f]	0.89 ± 0.01	
S126C	0.02	SS	apo[b]	−	dimer[f,g]		+
			Mn[c]	4741 ± 82 (65%)[e]	dimer[f,g]	0.95 ± 0.04	
Y174C	0.02	SS	apo[b]	−	dimer[g]		+
			Mn[c]	1123 ± 20 (28%)[e]	nd	0.99 ± 0.01	
S126C/Y174C	0.07	2×SS	apo[b]	−	dimer[g]		+
			Mn[c]	103 ± 1 (2%)[e]	nd	0.20 ± 0.01	
			Mn[d]	−	nd	0.05 ± 0.0	
E170C	0.02	SS	apo[b]	−	dimer[g]		+
			Mn[c]	44 ± 2 (0.6%)	nd	0.48 ± 0.005	
R72C/D147C/bBm	0.01		apo[b]	−	nd		+
			Mn[c]	6287 ± 70 (86%)	nd	0.89 ± 0.03	
H17C/N190C	0.02	SS	apo[b]	−	nd		+
			Mn[c]	8267 ± 232 (113%)	nd	1.02 ± 0.05	

[a] Based on the DTNB assay. [b] Before the metal uptake experiment. [c] After metal reconstitution. [d] After denaturation, renaturation, and reconstitution in the presence of Mn^{2+}. [e] Relative to WT MnSOD (7328 ± 216 units/mg). [f] Based on size exclusion chromatography. [g] Based on nonreducing SDS−PAGE. [h] Evaluated by Co^{2+} quenching in the fluorimetric metal uptake assay.

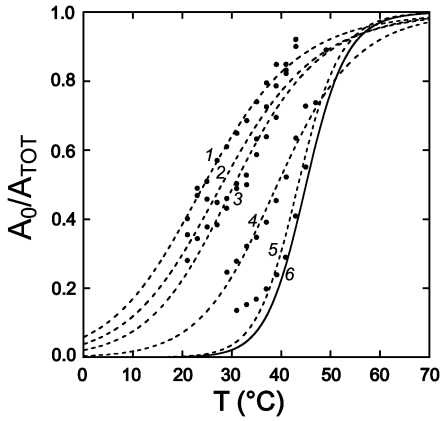

FIGURE 7: Temperature dependence of metal uptake for active site variants of MnSOD. Apoprotein (50 μg/mL) in 20 mM MOPS (pH 7) was analyzed by the fluorimetric metal uptake assay as described in Materials and Methods. Kinetic time courses were analyzed to extract the gating fraction in the fast phase (A_0/A_{TOT}) for each temperature and the temperature dependence fit to a two-state thermal melting curve: (1) apo-MnSOD Y34F, T_m = 24 °C; (2) apo-MnSOD Y34A, T_m = 28 °C; (3) apo-MnSOD H30A, T_m = 30 °C; (4) apo-MnSOD Y174F, T_m = 39 °C; (5) apo-MnSOD H171A, T_m = 43 °C; (6) WT apo-MnSOD, T_m = 45 °C.

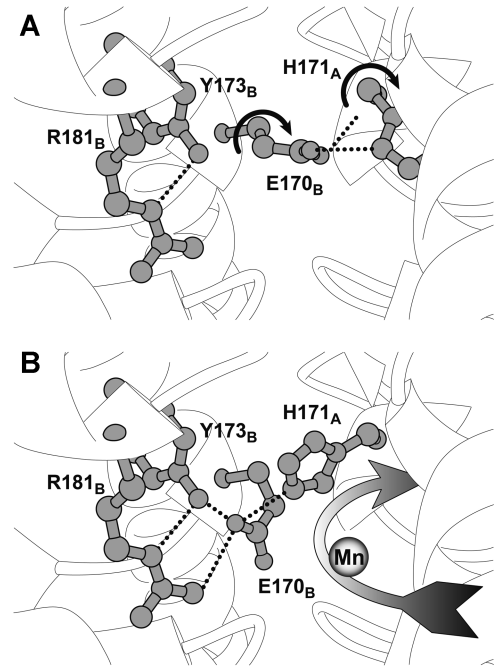

FIGURE 8: Proposed structural basis for the conformational gating transition. (A) Closed state model, stabilized by a hydrogen bond salt bridge between the interface-spanning glutamate ($Glu170_B$) and the active site residue ($His171_A$) within the opposing subunit. Based on the structure of the metalated MnSOD (PDB entry 1vew). Side chain dihedral rotations that generate the open state structure are indicated by the curved arrows. (B) Hypothetical model for the open state structure of apo-MnSOD. Reorientation of $Glu170_B$ glutamate within the conserved intersubunit channel is facilitated by formation of a salt bridge with the arginine residue ($Arg181_B$) and a hydrogen bond with tyrosine ($Tyr173_B$). Rotation of the $His171_A$ side chain, in turn, permits it to form a hydrogen bond with the carboxylate of $Glu170_B$. In the open conformation, a continuous channel is formed leading into the metal binding site from solution (Figure 9B).

subunits experience electrostatic repulsion when the sites are fully occupied, which is relieved when one of the metal ions dissociates.

Disulfide engineering thus provides clear evidence excluding subunit dissociation as the basis for apo-MnSOD metal binding and also excludes several domain interfaces from contributing to the process. However, the dramatic effect of several of the intersubunit cross-links on the metal binding reaction suggests that some motion at the subunit interface may be required for metal uptake to occur.

Active Site Variants. Residues surrounding the active site of EC MnSOD form an extensive hydrogen bonding web whose role in catalysis has previously been investigated by mutagenesis (*26*−*29*). Mutations have targeted the "substrate gateway" residues His30 and Tyr34 (H30A, Y34F, and Y34A) as well as the interface-spanning residue Tyr174 (Y174F). X-ray crystal structures have been determined for Mn complexes of several of these variants. To refine the apo-MnSOD metal binding mechanism and elucidate the structural basis for the conformational gating transition, the metal uptake behavior of these variants has been explored.

(i) H30A. His30 forms half of the substrate gateway (Figure 1) which is thought to restrict access to the active site metal ion in SOD, conferring substrate selectivity and possibly facilitating proton transfer steps in the redox turnover mechanism (*28*). The substrate gateway is also a barrier to metal binding, so displacement of the gateway residues might provide a pathway for entry of metal into the active site. In addition to its role as a gateway residue, His30 is also involved in a π-stacking interaction with His171 and forms a hydrogen bond with Tyr174. Replacement of His30 with alanine (MnSOD H30A) removes the steric bulk of the His side chain and at the same time disrupts interactions with His171 and Tyr174. The structure of the metallated Mn_2-MnSOD H30A protein has previously been reported (PDB entry 1io8) (*28*).

Apo-MnSOD H30A exhibits rapid metal uptake at 37 °C, characteristic of the open state behavior of WT apo-MnSOD. However, at lower temperatures, the biphasic metal uptake kinetics are restored (Figure 6, trace 4), associated with a sigmoidal temperature dependence (T_m = 30 °C) (Figure 7, curve 3). It is clear that while H30A substitution significantly perturbs the structural elements involved in the conformational gating process (shifting the closed−open equilibrium in favor of the open form) those features are still present in this variant. The pH dependence of the gating transition is retained but similarly shifted, with an apparent pK_a of 7.7 at 25 °C and a log-linear rate dependence slope ($-m$ = 0.7) (data not shown), indicating that the group responsible for the pH sensitivity of metal uptake is still present in this variant.

(ii) Y34A. Tyr34 combines with H30 to form the substrate gateway in MnSOD. As with MnSOD H30A, replacement of Tyr34 with alanine (MnSOD Y34A) is predicted to remove a significant steric barrier to access to the metal binding site, mimicking displacement of the side chain. However, Y34A substitution will also disrupt the extensive hydrogen bonding web surrounding the active site.

As observed for apo-MnSOD H30A, apo-MnSOD Y34A exhibits a perturbed biphasic metal binding reaction (Figure 6, trace 6), with the midpoint for the temperature-dependent metal uptake profile shifted to 28 °C (Figure 7, curve 2). Again, while strongly perturbed, the characteristic features of the gated metal uptake process appear to be preserved in this variant.

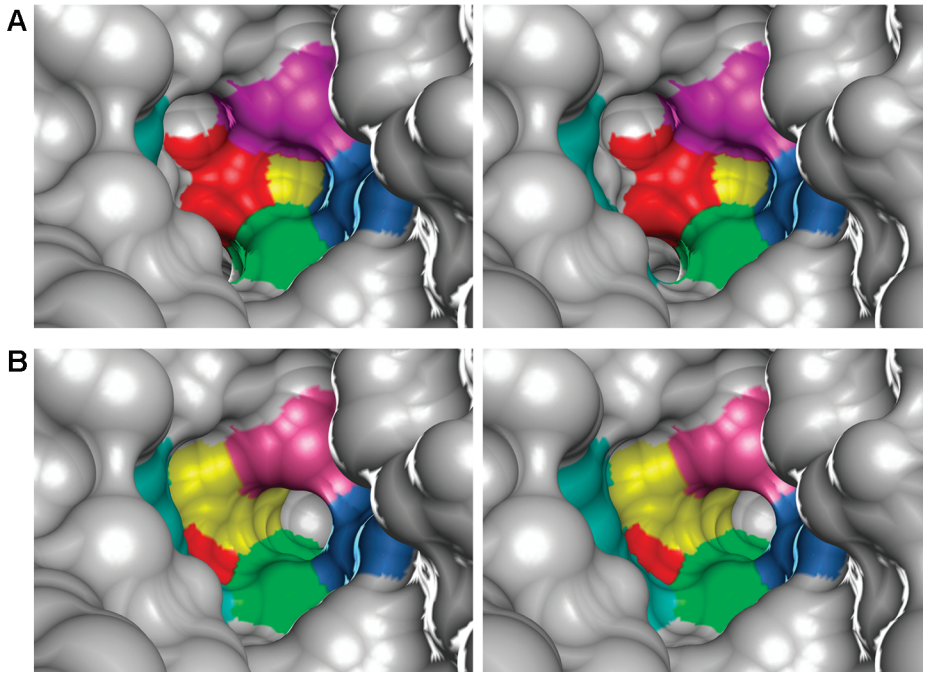

FIGURE 9: Proposed metal entry channel for apomanganese superoxide dismutase. (A) Stereoview molecular surface representation (1.4 Å probe radius) of the active site environment of native, metalated *E. coli* MnSOD, corresponding to the closed state apoprotein structure (Figure 8A), with the buried metal binding site lying behind the $His171_A$ side chain. The surface color reflects the contribution of specific residues. (B) Stereoview molecular surface view (1.4 Å probe radius) of the active site environment in the open state structure model (Figure 8B) from the same viewpoint as above, showing how reorientation of the side chains creates a metal entry channel leading from solution into the buried metal binding site. The surface color reflects the contribution of specific residues. Color code: magenta, $His30_A$; blue, $Tyr34_A$; green, $Trp169_A$; yellow, $His171_A$; red, $Glu170_B$; turquoise, $Arg181_B$. Rendered using Chimera (*13*). Based on PDB entry 1vew.

(iii) Y34F. Conservative replacement of Tyr34 with phenylalanine retains most of the steric bulk of the side chain, and the X-ray crystal structure of this variant (PDB entry 1en5) shows that the phenylalanine ring position is essentially superimposable with the Tyr34 ring it replaces; however, elimination of the Tyr34 hydroxyl group significantly disrupts the hydrogen bonding web around the active site (*27*). The metal uptake behavior of apo-MnSOD Y34F resembles that observed for other substrate gateway variants (H30A and Y34A), in that the biphasic conformational gating signature is preserved (Figure 6, trace 7) but shifted even more dramatically ($T_m = 24$ °C) (Figure 7, curve 1). This suggests the conformational gating transition is sensitive to the hydrogen bonding character of the substrate gateway residues, rather than their steric bulk. As with apo-MnSOD H30A, the pH dependence of the gating transition of apo-MnSOD Y34F is shifted to a lower-pH range with an apparent pK_a of 6.8 at 25 °C, although the kinetic sensitivity to pH is preserved ($-m = 0.6$) (data not shown).

All three mutational variants (H30A, Y34A, and Y34F) retain the metal cofactor after reconstitution and exhibit activity (data not shown) similar to that of the as-isolated metal complex reported previously (*27*−*29*). Interestingly, these variants appear to have a stronger effect on metal binding than on catalysis, suggesting that conservation of these residues may be driven to a significant extent by their contribution to the metal uptake process.

(iv) Y174F. Replacement of the subunit interface-spanning residue Tyr174 with Cys disulfide permits metal uptake to occur, although the uptake kinetics are significantly perturbed by the substitution (see above). Substitution of this residue with phenylalanine (MnSOD Y174F) has been shown to affect the structure of the protein at the subunit interface, as a result of eliminating a hydrogen bond with His30. The previously reported crystal structure of Mn_2-MnsSOD Y174F (PDB entry 1i0h, 1ixB, and 1ix9) indicates that Y174F substitution alters the orientation of the H30 ring and results in a local reorganization of the dimer interface (*29*). However, metal uptake by apo-MnSOD Y174F still exhibits conformational gating (Figure 6, trace 5) and is actually less dramatically perturbed compared to that of the other active site variants, with a T_m of 39 °C (Figure 7, curve 4).

(v) E170A. Removing the subunit interface-spanning Glu170 residue destabilizes the dimeric structure of EC MnsSOD, resulting in extensive dissociation into monomers (*26*) (Figure 4). Disruption of the dimer dramatically alters metal uptake, and this variant is characterized by rapid, monophasic metal binding kinetics (Figure 6, trace 11), similar to those observed for apo-MnSOD S126C SH.

(vi) H171A. His171 is the partner to Glu170 in the dimer-stabilizing salt bridge and serves as a ligand in the metal complex. Replacement with alanine (MnSOD H171A) does not have an effect on quaternary structure as dramatic as E170A substitution, since Glu170 also makes hydrogen bonding contacts with a backbone peptide in the opposing subunit, and MnSOD H171A is experimentally found to be dimeric in solution. Metal uptake by apo-MnSOD H171A is perturbed, but the kinetics are distinct from those observed for the other active site variants described above. The fast phase amplitude of the conformational gating transition is very small at 37 °C, yielding essentially monophasic metal uptake kinetics (Figure 6, trace 14) that are virtually independent of pH ($-m = 0.15$). In contrast to the pH dependence of metal uptake by WT apoprotein and H30A

and Y34F variants, where a proton molecularity approaches unity ($-m = 1.1$, 0.7, and 0.6, respectively), analysis of the pH dependence for apo-MnSOD H171A reflects loss of the proton ionization step in the metal uptake reaction of the variant protein, which is also seen for MnSOD E170C SS (see above). On the other hand, the temperature dependence of metal uptake is nearly identical to that of WT apo-MnSOD (Figure 7, curve 5). The H171A mutation thus appears to uncouple thermal and pH effects on metal binding by apo-MnSOD.

The properties of these active site variants allow the structural basis for the gating transition in apo-MnSOD to be more clearly defined. While the substrate gateway residues (His30 and Tyr34) represent the most obvious barrier to metal binding in the outer sphere of the metal binding site, their replacement with less bulky residues only perturbs, but does not eliminate, the characteristic biphasic kinetics and pH sensitivity of metal uptake by apo-MnSOD. The effects of these substrate gateway mutations are most likely indirect, acting through π-stacking and hydrogen bonding networks in the active site environment. Only apo-MnSOD E170C SS and apo-MnSOD H171A exhibit metal uptake kinetics lacking pH sensitivity. As discussed above (Biochemical Characterization of the Gating Transition), the pH dependence implicates a salt bridge in the protein in the conformational gating process, and the observed pK_a is consistent with deprotonation of a histidine−carboxylate ion pair in the closed → open transition, focusing attention on the interaction between Glu170 and His171.

A Model for the Conformational Gating Transition. The evidence accumulated in these studies suggests that the salt bridge between Glu170 and His171 plays a key role in the conformational gating transition of apo-MnSOD. However, if these residues are responsible for gating metal uptake, they must rearrange in the open state since they block access to the active site region in the metalated protein (Figure 1) that corresponds to the closed form of the apoprotein. Analysis of the metal uptake behavior of apo-MnSOD variants demonstrates that subunit dissociation is not required for metal binding, although some motion of the subunit interface appears to be involved in the gating transition, associated with a more subtle reorganization of the subunit interface. Inspection of the crystal structure of the metalated protein (PDB entry 1vew) suggests an alternative conformation that might represent the open form of the complex, generated by simple side chain torsions for Glu170 and His171 without any change in the peptide backbone (Figure 8). Rotation of the Glu170 side chain allows the carboxylate headgroup to ion pair with a pair of residues (Tyr173 and Arg181) which are highly conserved over Mn,Fe-SOD sequences yet have no recognized function. Reorientation of His171 can then proceed through simple rotation around the $C_\alpha-C_\beta$ bond, forming a hydrogen bond between the imidazole ring and the Glu170 carboxylate. While this alternative conformation has never been observed in any metalated SOD crystal structure, it is consistent with the evidence of a critical role for Glu170 and His171 in the conformational gating process, as well as the requirement for motion on the subunit interface for the gating transition to occur. Other residues in the active site environment (including His30 and Tyr34) are clearly important for determination of the relative stability of the alternative structures.

This model also accounts for the ready access of metal ions in solution to the metal binding site in the open state. Reorientation of the side chains opens a new channel into the buried binding site (Figure 9B), lined by substrate gateway residues (His30 and Tyr34) and metal gateway residues (Glu170, His171, Tyr173, and Arg181). The charge status of the residues in this open state is also favorable for metal entry through the channel. The Glu170 carboxylate (-1) neutralizes the $+1$ charge of the Arg181 guanidinium group, removing an electrostatic barrier for binding a metal cation, and the His171 side chain is deprotonated to a neutral imidazole in the open form. The proposed reorientation of His171 also permits coordination of the metal at NE2, which ligates the metal ion in the holoprotein, as it enters the metal entry channel. There is no obvious obstacle to this structural rearrangement, which occurs in a conserved channel that transects the dimer interface just below the Glu170−His171 salt bridge (Figure 9A) and previously had no known function. While it is difficult to evaluate all of the factors contributing to the relative stability of the open and closed conformations, their interconversion under mild conditions (temperature and pH) suggests that these two states are closely matched energetically.

CONCLUSIONS

Conformational gating of metal uptake by apo-MnSOD is a striking feature of the metal binding process reflecting unexpected dynamic features of the protein structure. Previous models that have been proposed for the open state of apo-MnSOD required large-scale reorganization of the protein structure, involving either subunit dissociation or domain separation. Both models are now excluded by studies of metal uptake by MnSOD variants in which those interfaces are constrained by covalent disulfide cross-linking. A detailed characterization of the properties of WT protein and mutational variants demonstrates that metal uptake by apo-MnSOD can occur under physiological conditions (temperature and pH) and provides new insight into the gating mechanism, leading to a model based on a localized conformational change that opens a metal entry channel into the active site. Two residues (Glu170 and His171) that lie on both domain and subunit interfaces are predicted to reorient, assisted by other residues in the active site environment, adopting an alternative conformation that removes the barriers to entry of metal into the active site. The residues involved are highly conserved over the entire superfamily of Mn,Fe-SOD structures, suggesting a universal mechanism controlling metal uptake by these proteins that may contribute to metal binding selectivity in vivo.

ACKNOWLEDGMENT

We thank Dr. Larry David, Dr. Debra McMillen, and Dr. John Klimeck of the Proteomics Core Facility (funded by the Oregon Opportunity and the National Institutes of Health) for their assistance.

REFERENCES

1. Kuchar, J., and Hausinger, R. P. (2004) Biosynthesis of metal sites. *Chem. Rev. 104*, 509–525.
2. Rosenzweig, A. C. (2002) Metallochaperones: Bind and deliver. *Chem. Biol. 9*, 673–677.

3. Culotta, V. C., Yang, M., and O'Halloran, T. V. (2006) Activation of superoxide dismutases: Putting the metal to the pedal. *Biochim. Biophys. Acta 1763*, 747–758.
4. Blokesch, M., Paschos, A., Theodoratou, E., Bauer, A., Hube, M., Huth, S., and Böck, A. (2002) Metal insertion into NiFe-hydrogenases. *Biochem. Soc. Trans. 30*, 674–680.
5. Dos Santos, P. C., Dean, D. R., Hu, Y., and Ribbe, M. W. (2004) Formation and insertion of the nitrogenase iron-molybdenum cofactor. *Chem. Rev. 104*, 1159–1173.
6. Gifford, J. L., Walsh, M. P., and Vogel, H. J. (2007) Structures and metal-ion-binding properties of the Ca^{2+}-binding helix−loop−helix EF-hand motifs. *Biochem. J. 405*, 199–221.
7. McCord, J. M. (1993) Oxygen-derived free radicals. *New Horiz. (Baltimore) 1*, 70–76.
8. Fridovich, I. (1995) Superoxide radical and superoxide dismutases. *Annu. Rev. Biochem. 64*, 97–112.
9. Parker, M. W., and Blake, C. C. (1988) Iron- and manganese-containing superoxide dismutases can be distinguished by analysis of their primary structures. *FEBS Lett. 229*, 377–382.
10. Yamakura, F., Kobayashi, K., Furukawa, S., and Suzuki, Y. (2007) In vitro preparation of iron substituted human manganese superoxide dismutase: Possible toxic properties for mitochondria. *Free Radical Biol. Med. 43*, 423–430.
11. Edwards, R. A., Baker, H. M., Whittaker, M. M., Whittaker, J. W., Jameson, G. B., and Baker, E. N. (1998) Crystal structure of *Escherichia coli* manganese superoxide dismutase at 2.1 Å resolution. *J. Biol. Inorg. Chem. 3*, 161–171.
12. Lah, M. S., Dixon, M. M., Pattridge, K. A., Stallings, W. C., Fee, J. A., and Ludwig, M. L. (1995) Structure-function in *Escherichia coli* iron superoxide dismutase: Comparisons with the manganese enzyme from *Thermus thermophilus*. *Biochemistry 34*, 1646–1660.
13. Pettersen, E. F., Goddard, T. D., Huang, C. C., Couch, G. S., Greenblatt, D. M., Meng, E. C., and Ferrin, T. E. (2004) UCSF Chimera: A Visualization System for Exploratory Research and Analysis. *J. Comput. Chem. 25*, 1605–1612.
14. Mizuno, K., Whittaker, M. M., Bächinger, H. P., and Whittaker, J. W. (2004) Calorimetric studies on the tight binding metal interactions of *Escherichia coli* manganese superoxide dismutase. *J. Biol. Chem. 279*, 27339–27344.
15. Ose, D. E., and Fridovich, I. (1979) Manganese-containing superoxide dismutase from *Escherichia coli*: Reversible resolution and metal replacements. *Arch. Biochem. Biophys. 194*, 360–364.
16. Beyer, W. F., Jr., and Fridovich, I. (1991) *In vivo* competition between iron and manganese for occupancy of the active site region of the manganese-superoxide dismutase of *Escherichia coli*. *J. Biol. Chem. 266*, 303–308.
17. Whittaker, M. M., and Whittaker, J. W. (1999) Thermally triggered metal binding by recombinant *Thermus thermophilus* manganese superoxide dismutase, expressed as the apo-enzyme. *J. Biol. Chem. 274*, 34751–34757.
18. Whittaker, M. M., and Whittaker, J. W. (2000) Recombinant superoxide dismutase from a hyperthermophilic archaeon *Pyrobaculum aerophilum*. *J. Biol. Inorg. Chem. 5*, 402–408.
19. Whittaker, M. M., Mizuno, K., Bächinger, H. P., and Whittaker, J. W. (2006) Kinetic analysis of the metal binding mechanism of *Escherichia coli* manganese superoxide dismutase. *Biophys. J. 90*, 598–607.
20. Jameson, G. B., Adams, J. J., Hempstead, P. D., Anderson, B. F., Morgenstern-Badarau, I., Whittaker, J. W., and Baker, E. N. (2003) Superoxide dismutases from hyperthermophiles: Clues to metal-ion specificity. *J. Inorg. Biochem. 96*, 70.
21. Lee, S., Sawaya, M. R., and Eisenberg, D. (2003) Structure of superoxide dismutase from *Pyrobaculum aerophilum* presents a challenging case in molecular replacement with multiple molecules, pseudo-symmetry and twinning. *Acta Crystallogr. D59*, 2191–2199.
22. Miller, E. M., and Nickoloff, J. A. (1995) *Escherichia coli* electrotransformation. *Methods Mol. Biol. 47*, 105–113.
23. Datsenko, K. A., and Wanner, B. L. (2000) One-step inactivation of chromosomal genes in *Escherichia coli* K-12 using PCR products. *Proc. Natl. Acad. Sci. U.S.A. 97*, 6640–6645.
24. Liu, P., Jenkins, N. A., and Copeland, N. G. (2003) A highly efficient recombineering-based method for generating conditional knockout mutations. *Genome Res. 13*, 476–484.
25. Gao, B., Flores, S. C., Bose, S. K., and McCord, J. M. (1996) A novel *Escherichia coli* vector for oxygen-inducible high level expression of foreign genes. *Gene 176*, 269–270.
26. Whittaker, M. M., and Whittaker, J. W. (1998) A glutamate bridge is essential for dimer stability and metal selectivity in manganese superoxide dismutase. *J. Biol. Chem. 273*, 22188–22193.
27. Whittaker, M. M., and Whittaker, J. W. (1997) Mutagenesis of a proton linkage pathway in *Escherichia coli* manganese superoxide dismutase. *Biochemistry 36*, 8923–8931.
28. Edwards, R. A., Whittaker, M. M., Whittaker, J. W., Baker, E. N., and Jameson, G. B. (2001) Outer sphere mutations perturb metal reactivity in manganese superoxide dismutase. *Biochemistry 40*, 15–27.
29. Edwards, R. A., Whittaker, M. M., Whittaker, J. W., Baker, E. N., and Jameson, G. B. (2001) Removing a hydrogen bond in the dimer interface of *Escherichia coli* manganese superoxide dismutase alters structure and reactivity. *Biochemistry 40*, 4622–4632.
30. Quijano, C., Hernandez-Saavedra, D., Castro, L., McCord, J. M., Freeman, B. A., and Radi, R. (2001) Reaction of peroxynitrite with Mn-superoxide dismutase. Role of the metal center in decomposition kinetics and nitration. *J. Biol. Chem. 276*, 11631–11638.
31. Beyer, W. F., Jr., Reynolds, J. A., and Fridovich, I. (1989) Differences between the manganese- and the iron-containing superoxide dismutases of *Escherichia coli* detected through sedimentation equilibrium, hydrodynamic, and spectroscopic studies. *Biochemistry 28*, 4403–4409.
32. Lowry, O. H., Rosebrough, N. J., Farr, A. L., and Randall, R. J. (1951) Protein measurement with the Folin phenol reagent. *J. Biol. Chem. 193*, 265–275.
33. McCord, J. M., and Fridovich, I. (1969) Superoxide dismutase. An enzymic function for erythrocuprein (hemocuprein). *J. Biol. Chem. 244*, 6049–6055.
34. Riddles, P. W., Blakeley, R. L., and Zerner, B. (1983) Reassessment of Ellman's reagent. *Methods Enzymol. 91*, 49–60.
35. Means, G. E., and Feeney, R. E. (1971) *Chemical Modification of Proteins*, pp 157−158, Holden-Day, New York.
36. Kim, J.-S., and Raines, R. T. (1995) Dibromobimane as a fluorescent cross-linking reagent. *Anal. Biochem. 225*, 174–176.
37. Markley, J. L. (1975) Observation of histidine residues in proteins by nuclear magnetic resonance spectroscopy. *Acc. Chem. Res. 8*, 70–80.
38. Loudon, G. M. (1991) Mechanistic interpretation of pH-rate profiles. *J. Chem. Educ. 68*, 973–984.
39. Thurlkill, R. L., Grimsley, G. R., Scholtz, J. M., and Pace, C. N. (2006) pK values of the ionizable groups in proteins. *Protein Sci. 15*, 1214–1218.
40. Anderson, D. E., Becktel, W. J., and Dahlquist, F. W. (1990) pH-induced denaturation of proteins: A single salt bridge contributes 3−5 kcal/mol to the free energy of folding of T4 lysozyme. *Biochemistry 29*, 2403–2408.
41. Frey, P. A., Whitt, S. A., and Tobin, J. B. (1994) A low-barrier hydrogen bond in the catalytic triad of serine proteases. *Science 264*, 1927–1930.
42. Matsumura, M., and Matthews, B. W. (1991) Stabilization of functional proteins by introduction of multiple disulfide bonds. *Methods Enzymol. 202*, 336–356.
43. Tomishige, M., and Vale, R. D. (2000) Controlling kinesin by reversible disulfide cross-linking: Identifying the motility-producing conformational change. *J. Cell Biol. 151*, 1081–1092.
44. Schultz-Heienbrok, R., Maier, T., and Sträter, N. (2004) Trapping a 96° domain rotation in two distinct conformations by engineered disulfide bridges. *Protein Sci. 13*, 1811–1822.
45. Thornton, J. M. (1981) Disulfide bridges in globular proteins. *J. Mol. Biol. 151*, 261–287.
46. Richardson, J. S. (1981) The anatomy and taxonomy of protein structures. *Adv. Protein Chem. 34*, 167–339.
47. Guzman, L. M., Belin, D., Carson, M. J., and Beckwith, J. (1995) Tight regulation, modulation, and high-level expression by vectors containing the arabinose pBAD promoter. *J. Bacteriol. 177*, 4121–4130.
48. Green, N. S., Reisler, E., and Houk, K. N. (2001) Quantitative evaluation of the lengths of homobifunctional protein cross-linking reagents used as molecular rulers. *Protein Sci. 10*, 1293–1304.
49. Bunting, K. A., Cooper, J. B., Tickle, I. J., and Young, D. B. (2002) Engineering of an intersubunit disulfide bridge in the iron superoxide dismutase from *Mycobacterium tuberculosis*. *Arch. Biochem. Biophys. 397*, 69–76.

BI8015636